JOURNAL OF MATERIALS SCIENCE 27 (1992) 3685–3692

Electrical properties of polycrystalline PTCR barium titanate

M. A. A. ISSA
Materials Study Group, Department of Physics, Faculty of Science, King Saud University, PO Box 2455, Riyadh 11451, Saudi Arabia

Semiconducting n-type barium titanate with a positive temperature coefficient of resistance (PTCR) has been made by doping $BaTiO_3$ with 0.4 mol% Ho_2O_3. The d.c. resistivity, a.c. resistivity (1.2 kHz) and relative permittivity (1.2 kHz) at different temperatures between room temperature and 523 K have been measured. The high relative permittivity and the PTCR effect are attributed to the existence of potential barriers at the grain boundaries as proposed by Heywang. The height of the potential barrier has been calculated as a function of temperature on the basis of the Heywang model, using the measured resistivity versus temperature and relative permittivity versus temperature above the Curie temperature. Several different kinds of electrode have been used to study the effect of the contact on measurements of resistivity and relative permittivity.

1. Introduction

Semiconducting n-type polycrystalline barium titanate can be prepared by partially substituting Ba^{2+} by a small amount of triavalent cations such as rare-earth elements, or Ti^{4+}, by pentavalent cations such as Nb^{5+} and Sb^{5+}. The defects are compensated by free electrons in the conduction band. The doped $BaTiO_3$, sintered in air, exhibits a very high relative permittivity, compared to the relative permittivity of undoped $BaTiO_3$, and an anomalous sharp increase in resistivity known as a positive temperature coefficient of resistivity (PTCR) above the ferroelectric para-electric transition temperature [1–45].

Various models have been proposed to interpret the relative permittivity and PTCR behaviour in doped $BaTiO_3$ [3, 8, 9, 12–18]. The most satisfactory model that explains the PTCR is the Heywang model [3, 9]. The effects are attributed to the existence of potential barriers at the grain boundary regions, thought to be caused by acceptor-type surface states. This model attributes the shape of the PTCR above the Curie point to a rapid decrease in relative permittivity, which leads to a sharp rise in the height of the grain boundary potential barrier. Jonker [8] has modified this model by proposing that the spontaneous polarization of the ferroelectric phase at the end of alternate domains below the Curie temperature could effectively compensate the surface-state charge, eliminating the potential barrier height, and hence lead to the observed low resistivity of this material.

Extensive investigations have been done by many workers to study the effects of sintering conditions [20–28], porosity [29, 30] and defect structure on the PTCR and relative permittivity of doped $BaTiO_3$ [31–38]. The electrical properties of semiconducting ceramics have been found to be very sensitive to the nature of the electrode materials [39–43].

Measurements of relative permittivity $\varepsilon_m(T)$, resistivity $\rho(T)$, loss tangent ($\tan\delta$) and complex impedance analysis at different temperatures for different electrodes are reported here. The relation between $\rho(T)$ and $\varepsilon_m(T)$, and the values of the potential barrier height at different temperatures, are interpreted in terms of the Heywang model.

2. Experimental procedure

2.1. Sample preparation

$BaTiO_3$ doped with 0.4 mol% Ho_2O_3 was prepared from the proper proportions of $BaCO_3$ (99.5% pure), TiO_2 (99.8% pure) and Ho_2O_3 (99.9% pure) powders using conventional ceramic methods. The weighed powders were mixed and ground, in a medium of ethanol, in a planetary agate ball-mill for 1.5 h. After being dried, the powder was calcined at 1150 °C for 6 h in an alumina crucible in a muffle furnace using a heating rate of 5 °C min^{-1}. The calcined powder was milled again for 4 h and dried. In order to obtain compact pellets, powder with a small amount of PVA was pressed at a pressure of $\simeq$ 200 MPa. Disc-type samples of 13 mm diameter were obtained. Each sample was first heated to 500 °C for 6 h to eliminate the PVA and subsequently sintered at 1360 °C for 6 h using rates of heating and cooling back to room temperature of 2 °C min^{-1}. The sintered pellets shrunk in size to around 11 mm diameter. These were polished using 3 μm alumina powder on both sides to get highly parallel surfaces of 1.5 mm separation. The observed colour of samples under investigation (0.4 mol% Ho_2O_3) was dark blue.

0022–2461

For electrical measurements, four types of electrode were deposited on both sides of the cleaned disc samples. Ag, Au and Ni electrodes were made by evaporation on to the disc surfaces. Electrodes from In–Ga alloy (1:2 ratio) were applied by rubbing on the surfaces.

2.2. Measurements

Measurements of $\varepsilon_m(T)$, $\rho(T)$, $\tan\delta$ (at 1.2 kHz and 0.5 V) and the frequency dependence of the impedance were carried out in the range 20 Hz to 300 kHz by a Precision Inductance Analyzer 3245 (Wayne Kerr). D.c. resistance of the specimen was measured using a d.c. current source (Hewlett Packard 6186 C), a digital electrometer (Keithly 616) for measuring the current and a digital multimeter (Keithly 177) for measuring the voltage across the sample. The measurements were made from room temperature to 523 K, using a digital thermometer (Keithly 871) with a K-type thermocouple. The temperatures were controlled by a temperature controller (RKC MB-55) with $\pm$ 1 K accuracy.

X-ray diffraction (XRD) was used to determine the lattice constants of the crystal structure of the specimen.

The grain size in the final ceramic was estimated by the use of SEM (Jeol JSM-T 3308) of as-fired surfaces and fracture surfaces of the same sample.

3. Results and discussion

3.1. General

The X-ray powder diffraction data for undoped $BaTiO_3$ and $BaTiO_3$ doped with 0.4 mol % Ho_2O_3 were almost identical. Both showed a tetragonal structure and no additional phase is observed.

The formation of microstructure of the specimen is as shown in Fig. 1. The average grain sizes are 10 μm for $BaTiO_3$ doped with 0.4 mol % Ho_2O_3 and 57 μm for $BaTiO_3$. It is noted from these two values that the grain size of doped samples is much smaller than for undoped $BaTiO_3$. This behaviour indicates the grain growth inhibition by addition of Ho. This result agrees with previous work on $BaTiO_3$ doped with Ho [35] or with other rare-earth materials [45–47].

The density was found to be 95% of the theoretical value.

3.2. The effect of electrode material

Variations of the resistivity $\rho(T)$, relative permittivity $\varepsilon_m(T)$ and loss tangent ($\tan\delta$) for 0.4 mol % Ho_2O_3-doped $BaTiO_3$, at 1.2 kHz as a function of temperature using four different electrodes for the same specimen, are shown in Fig. 2. Fig. 3 shows the dependence of d.c. resistivity $\rho(T)$ on temperature for the same specimen with different electrodes. It can be seen from Figs 2 and 3 that $\rho(T)$, $\varepsilon_m(T)$ and $\tan\delta$ are sensitive to the nature of the electrode material. The resistivity $\rho(T)$, using evaporated Ag electrodes, is larger than those with other electrodes, especially between room temperature and the ferroelectric–paraelectric transition temperature (the Curie temperature T_C). As a result of this behaviour $\varepsilon_m(T)$ increased and $\tan\delta$ decreased following the temperature-dependent equation

$$1/\rho(T) = \omega\varepsilon_o\varepsilon_m(T)\tan\delta$$

where ω is the angular frequency and ε_o is the permittivity in a vacuum. Above T_C the relative permittivity decreases as a function of temperature in accordance with the Curie–Wiess law, while the resistivity increases and $\tan\delta$ decreases for all electrodes. Using an evaporated Au electrode we obtained similar values at high temperatures for $\rho(T)$, $\varepsilon_m(T)$ and $\tan\delta$ but in the range from room temperature to the Curie temperature the values are slightly different from these for an Ag electrode. Coating with In–Ga (1:2 ratio) alloy and evaporating Ni as electrodes gave similar results, but different from the results obtained with Ag and Au electrodes. For example, the minimum resistance was equal to 25 Ω with In–Ga electrodes whereas in the case of Ag it was 125 Ω. This value is smaller than those reported by other investigators [40, 43] who used Ag electrodes. They have reported that the resistivity of the specimen with Ag electrodes is very high and the PTCR effect is seldom observed. They used silver paste which contains some low-melting glass to facilitate bonding of the Ag electrode, which may have caused the extra high resistance.

The high resistivity of samples with Ag and Au electrodes resulted from an interfacial layer between the surface of the electrode and the surface of the

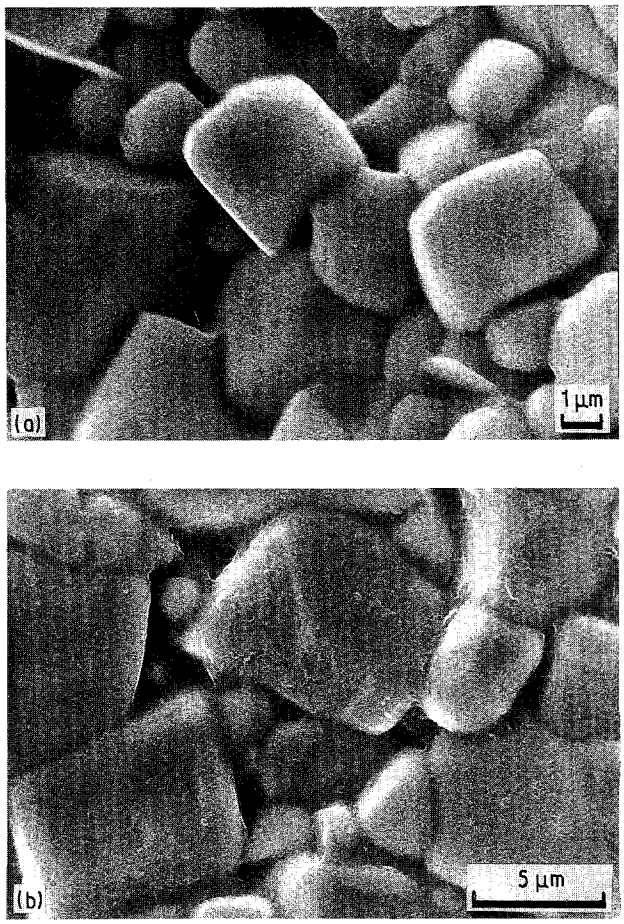

Figure 1 Scanning electron micrographs of (a) as-sintered surface and (b) fracture surface of $BaTiO_3$ doped with 0.4 mol % Ho_2O_3.

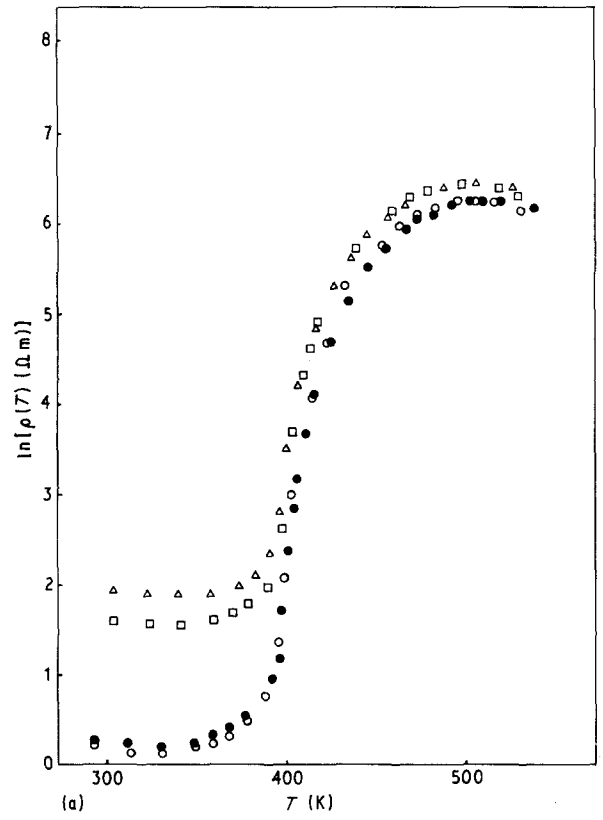

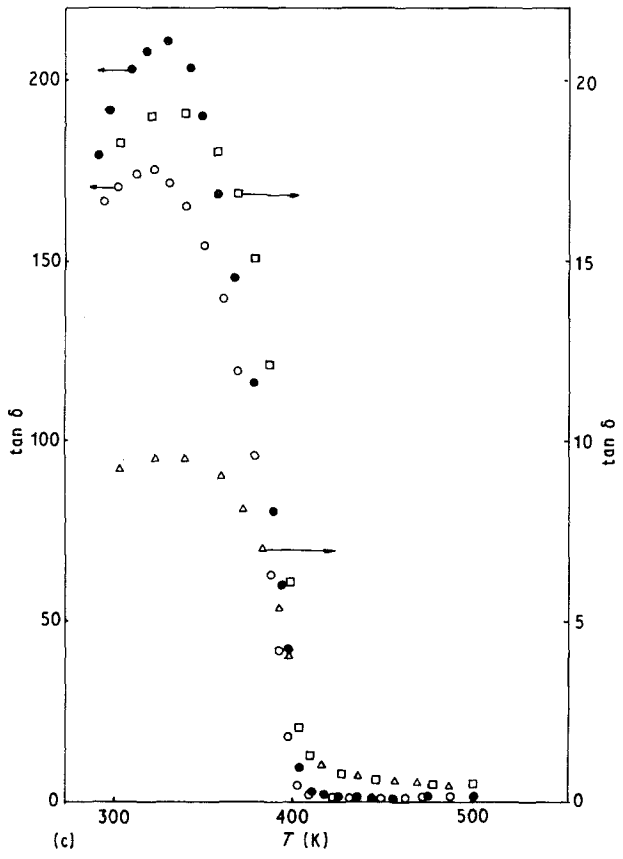

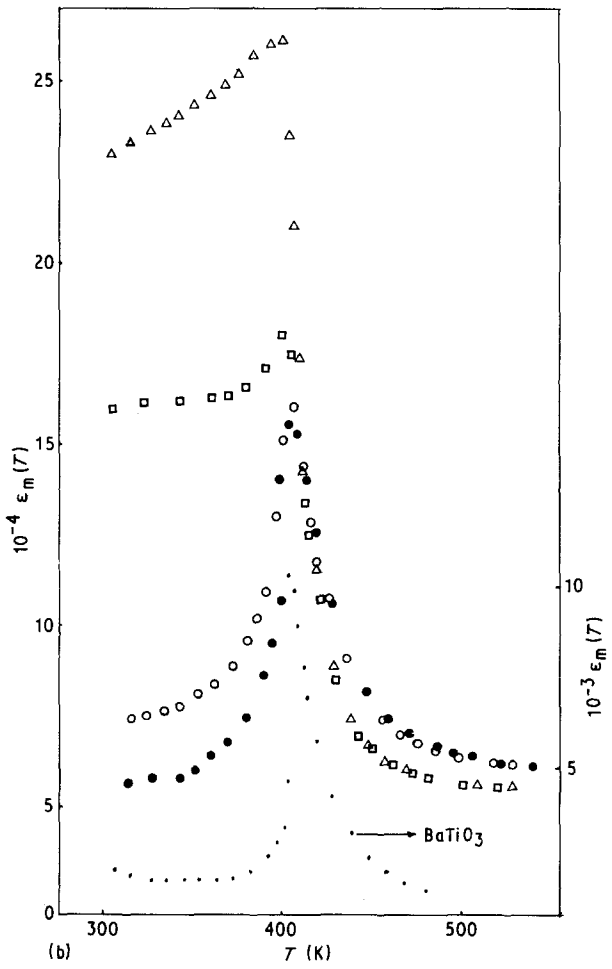

Figure 2 Temperature dependence of measured (a) resistivity, (b) relative permittivity, (c) tan δ for 0.4 mol % Ho_2O_3 doped $BaTiO_3$ with different electrodes: (△) Ag, (□) Au, (○) Ni and (●) In–Ga at 1.2 kHz; (b) also shows (·) the relative permittivity of $BaTiO_3$ at 1.2 kHz with Ni electrodes.

specimen, i.e. the contact resistance. The specimens with Ag and Au electrodes contain two types of depletion layer [41, 43] in addition to free electrons generated in the grains. One type of layer is formed at the grain boundary regions between the grains during the processing of the material, and the other between each electrode and the surface of the specimen.

Complex impedance plane plot analysis is quite a useful technique for determination of the resistance of conductive grains, grain boundaries and electrode interfaces. Generally, plotting the real part of the impedance (Z_1) versus the imaginary part (Z_2) at different frequencies for n-type $BaTiO_3$ ceramics [27, 40, 41] shows two semicircles corresponding to the grain boundary, at high frequency, and the electrode interface, at low frequency. Fig. 4 shows plots of Z_1 and Z_2 for In–Ga and Ag electrodes at different temperatures. At low temperature two semicircles were observed, corresponding to the grain boundaries (the small semicircle) and the electrode interfaces (the large semicircle) in the range of frequency examined with Ag electrodes. Above the Curie temperature the resistance of the grain boundaries increases as the temperature increases (PTCR) and hence the semicircle belonging to the grain boundaries increases. At high temperatures the two semicircles become mixed and only one semicircle is observed. For the In–Ga electrodes only one semicircle was obtained corresponding to the grain boundaries, which gets bigger with increase of the temperature. The estimated resistance, from the intercepts of the arcs on the real axis at low frequency for Ag electrodes, is higher than that

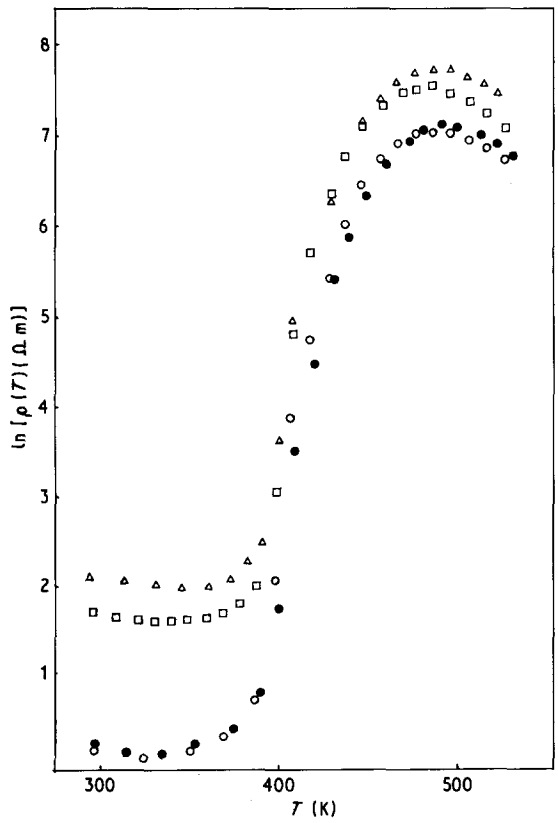

Figure 3 Temperature dependence of d.c. resistivity for 0.4 mol % Ho_2O_3 doped $BaTiO_3$ with different electrodes: (△) Ag, (□) Au, (○) Ni and (●) In–Ga.

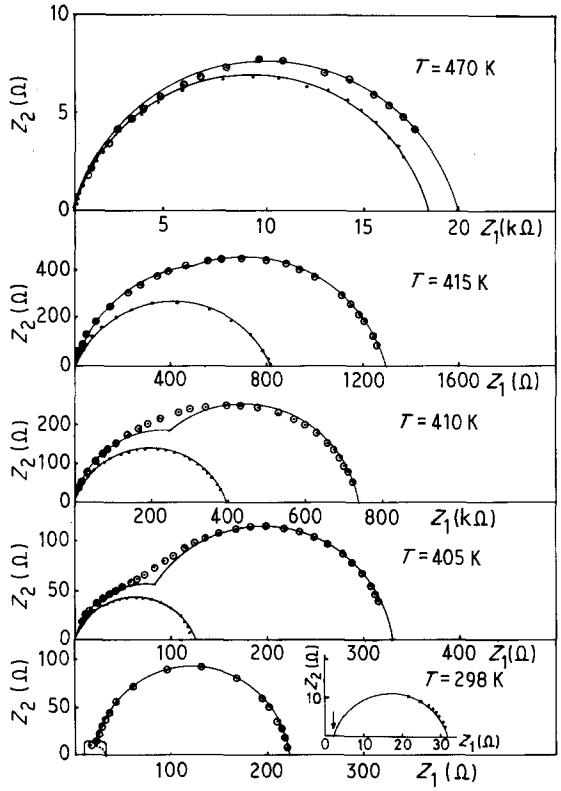

Figure 4 Complex plots of 0.4 mol % Ho_2O_3 doped $BaTiO_3$ at different temperatures with two kinds of electrode: (·) In–Ga and (⊙) Ag.

with In–Ga electrodes. The difference between the two values is due to the resistance of the electrode interfaces between the two faces of the material and the Ag electrodes. At room temperature the contact resistance of the Ag electrodes is about 200 Ω. The contact resistance of Au (200–500 Ω), In–Ga (≃ 0.7 Ω) and Ni (≃ 1 Ω) have been calculated by other workers [41] by using the same method and thickness variation of the samples. The grain resistance can be estimated from the intercept of the arc at high frequency, which is indicated by an arrow in Fig. 4. This resistance is about 2.5 Ω, and a similar value has been found by other investigators [38, 40].

Using coated In–Ga alloy and evaporated Ni we obtain suitable electrodes for the study of the PTCR effect in semiconducting $BaTiO_3$, due to the formation of a low ohmic contact with the material. The evaporated Ag and Au electrodes are non-ohmic contact electrodes due to the formation of high resistance with the semiconducting $BaTiO_3$. This resistance gives better dielectric properties; the relative permittivity is very high with an order of magnitude of about 10 and a relatively low loss tangent, as shown in Fig. 2.

3.3. Dependence of potential barrier height on temperature

The temperature dependence of the measured relative permittivity $\varepsilon_m(T)$ of doped and undoped $BaTiO_3$ at 1.2 kHz, using Ni electrodes, is as shown in Fig. 2b. They exhibit similar behaviour; nevertheless, the value of $\varepsilon_m(T)$ for the doped material shows values about two orders of magnitude higher than those of the undoped $BaTiO_3$ ceramic. Above the Curie temperature, the dependence of $\varepsilon_m(T)$ for pure $BaTiO_3$ usually follows a Curie–Weiss law which may be written as [49, 50]

$$\varepsilon_m(T) = \frac{C}{T - T_0} \quad (1)$$

or

$$\varepsilon_m(T) = \varepsilon_L + \frac{C}{T - T_0} \quad (2)$$

where C is the Curie constant, T_0 is the extrapolated Curie point and ε_L is the part of relative permittivity independent of temperature.

Fig. 5 shows the dependence of $1/\varepsilon_m(T)$ on temperature; for undoped $BaTiO_3$ the Curie–Weiss law (Equation 1) is obeyed where the calculated constants are $C = (1.44 \times 10^5)$ K and $T_0 = 383$ K. These values compare well with the results of other investigators [44, 49]. The dependence of $1/\varepsilon_m(T)$ on temperature of doped (0.4 mol % Ho_2O_3) $BaTiO_3$ (Fig. 5) shows that the Curie–Weiss law is obeyed within a small range of temperature above T_0 which is less than the range of temperature for pure $BaTiO_3$. The constants C and T_0 were measured and found to be (6.53×10^6) K and 363 K. There is another region of linearity at higher temperature with a smaller slope; the same behaviour has been noticed by other investigators [36].

With the value of $T_0 = 383$ K, $\varepsilon_m(T)$ versus $1/(T - T_0)$ is plotted in Fig. 6 by using the modified Curie–Weiss law of Equation 2. Linear plots were

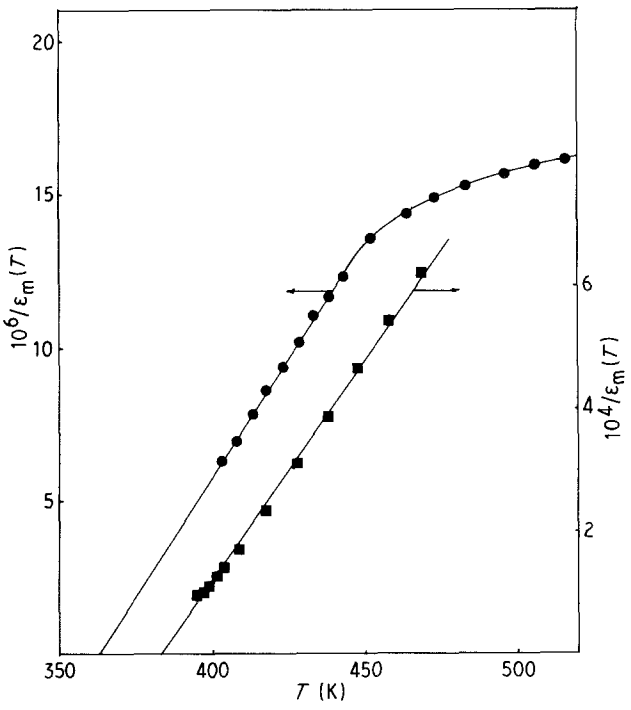

Figure 5 Reciprocal of the relative permittivity as a function of temperature (the Curie–Weiss Equation 1) of (●) $BaTiO_3$ doped with 0.4 mol % Ho_2O_3 and (■) $BaTiO_3$.

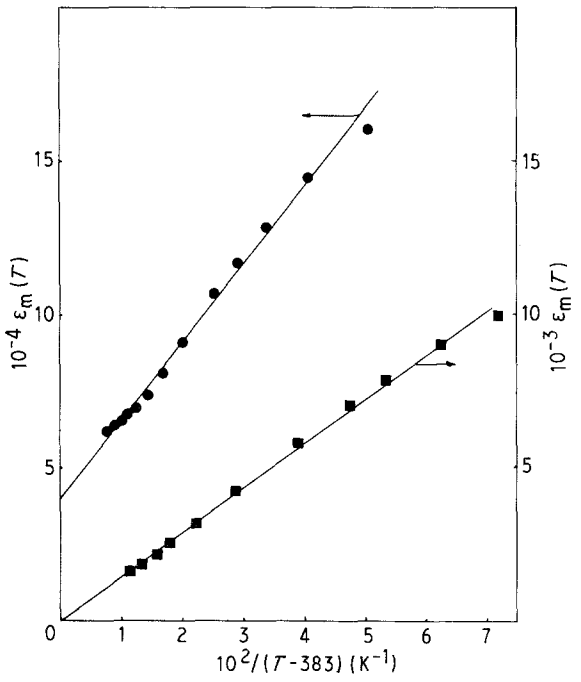

Figure 6 Relative permittivity versus $1/(T\text{-}383)$ the Curie–Weiss Equation 2) of (■) $BaTiO_3$ and (●) $BaTiO_3$ doped with 0.4 mol % Ho_2O_3.

obtained for doped and undoped $BaTiO_3$. For pure $BaTiO_3$ the values of C and T_0 are the same as calculated above and ε_L, which was obtained by extrapolation to infinite temperature, is very small (almost zero) which may be attributed to the contribution of electronic polarizability [49, 50]. For doped $BaTiO_3$, the values of C, T_0 and ε_L were obtained using Fig. 6 and were found to be (2.5×10^6) K, 383 K and 4×10^4, respectively.

The temperature dependence of measured resistivity $\rho(T)$, for d.c. and a.c. (at 1.2 kHz), is as shown in Figs 2a and 3. $\rho(T)$ for d.c. is higher than the a.c. values and it shows strong frequency dispersion [1, 48].

According to the model of Heywang which explains the PTCR effect [3, 9], the increase of resistivity above the Curie temperature is caused by potential barriers at the grain boundary. The relation between the resistivity $\rho(T)$ and the height of the potential barrier $e\phi(T)$ at temperature T is given by [9]

$$\rho(T) = \rho_0 \exp[e\phi(T)/kT] \tag{3}$$

and

$$e\phi(T) = \frac{e^2 N_d}{2\varepsilon_L(T)\varepsilon_o} x^2 \tag{4}$$

where e is the charge of electron, $\varepsilon_L(T)$ is the relative permittivity at the grain boundary layer at temperature T, ρ_0 is a constant, k is the Boltzmann constant and x is the width of the grain boundary which can be given as

$$x = \frac{n_s(T)}{2N_d} \tag{5}$$

where $n_s(T)$ is the temperature dependence of the density of occupied acceptor states. $n_s(T)$ is given by the equation [9]

$$n_s(T) = N_s\left[1 + \exp\left(\frac{E_F + e\phi - E_s}{kT}\right)\right]^{-1} \tag{6}$$

where N_s is the total acceptor density, E_s is the acceptor energy and E_F is the Fermi energy:

$$E_F = kT \ln(N_0/N_d)$$
$$N_0 = (1.56 \times 10^{28})\ m^{-3} \tag{7}$$

where N_0 is the number of Ti ions per m^3 (the effective density of states) [8]. N_d can be calculated from the relation [38]

$$N_d = 1/e\mu\rho_g$$

where μ is the electron mobility and equal to $(5 \times 10^{-5})\ m^2\ V^{-1}\ s^{-1}$ [38]; ρ_g is the bulk resistivity which can be calculated from the resistance of the bulk (2 Ω) and the sample dimensions. This gives for N_d a value of $(1.39 \times 10^{24})\ m^{-3}$. These results agree fairly well with those of other investigators [33, 36].

In order to describe the PTCR effect by using the Heywang model according to the measured (apparent) resistivity $\rho(T)$ and measured relative permittivity $\varepsilon_m(T)$ of the sample under investigation, a small modification of the theory was necessary. Following the modification of Kuwabara [30] and Al-Allack *et al.* [36] the relation between $\varepsilon_m(T)$ and $\varepsilon_L(T)$ is written as

$$\varepsilon_m(T) = \varepsilon_L(T)\frac{d}{2x} \tag{8}$$

where d is the average grain size (about 10 μm). Substituting Equations 8 and 5 into Equation 4 one can get

$$e\phi(T) = e^2 n_s(T) d/8\varepsilon_o\varepsilon_m(T) \tag{9}$$

Equation 9 shows that $e\phi(T)$ is inversely dependent on the measured $\varepsilon_m(T)$, assuming that N_d and x

are constants and $n_s(T)$ is constant within the range of temperature from T_0 to T_m (Fig. 2a). In this case the PTCR effect may be described by substituting Equation 9 into Equation 3 to get the equation

$$\rho(T) = \rho_0 \exp\left(\frac{G}{\varepsilon_m(T)T}\right) \quad (10)$$

or

$$\ln[\rho(T)] = \ln\rho_0 + \frac{G}{\varepsilon_m(T)T} \quad (11)$$

where

$$G = e^2 n_s(T) d/8\varepsilon_0 k \quad (12)$$

The plot of experimental results of $\ln[\rho(T)]$ versus $1/\varepsilon_m(T)T$ (Fig. 7) shows a straight line within the range of temperature between T_0 and T_m for the a.c. and d.c. measurements of $\rho(T)$. The values of the constants G and ρ_0 have been calculated from the slope and the intercept of the straight line with $\rho(T)$ and found to be

$$\rho_0 = 1.3\,\Omega\text{m} \qquad G = (2.15\times10^8)\,\text{K}$$

for d.c. measurements of $\rho(T)$ and

$$\rho_0 = 2.12\,\Omega\text{m} \qquad G = (1.7\times10^8)\,\text{K}$$

for a.c. measurements of $\rho(T)$. Using the value of G and Equation 12, the density of occupied acceptor states $n_s(T)$ could be calculated and found to be $(8.2\times10^{17})\,\text{m}^{-2}$ for d.c. measurements of $\rho(T)$ and $(6.5\times10^{17})\,\text{m}^{-2}$ for a.c. measurements of $\rho(T)$ at 1.2 kHz.

From Equations 3 and 10, $e\phi(T)$ can be written as

$$e\phi(T) = \frac{kG}{e\varepsilon_m(T)} \quad (13)$$

Fig. 8 shows the calculated $e\phi(T)$ at different temperatures. The data points of $e\phi(T)$, with d.c. and a.c. $\rho(T)$, lie on two straight lines both of which, when extrapolated, meet the axis of temperature at the Curie temperature T_0. This result confirms the validity of the Heywang model.

Attempts have been made to fit the experimental $\rho(T)$ with the theoretical model by solving numerically Equations 6, 7 and 13 and the equation

$$\rho(T) = \rho_0 \exp\left(\frac{e^2 n_s(T) d}{8kT\varepsilon_0\varepsilon_m(T)}\right) \quad (14)$$

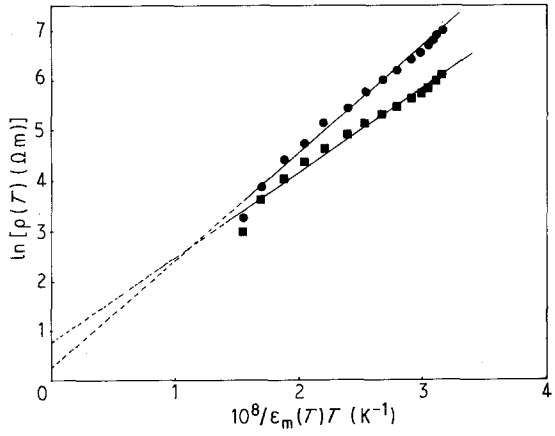

Figure 7 In $[\rho(T)]$ versus $1/\varepsilon_m(T)T$ for $BaTiO_3$ doped with 0.4 mol % Ho_2O_3 for (■) a.c. $\rho(T)$ and (●) d.c. $\rho(T)$.

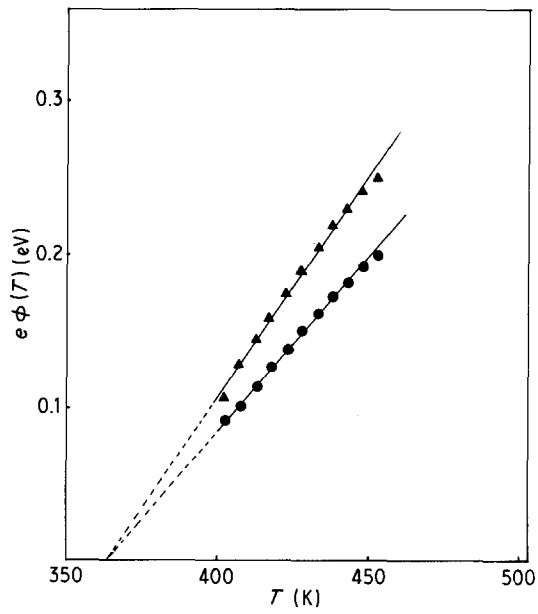

Figure 8 Temperature dependence of potential barrier height with (▲) d.c. $\rho(T)$ and (●) a.c. $\rho(T)$.

The theoretical dependence of $\varepsilon_m(T)$ on temperature has been given by the Curie–Weiss law (Equations 1 and 2). Different values of acceptor energies E_s and acceptor-state densities N_s have been used to get a better fit between theoretical and experimental values of d.c. and a.c. $\rho(T)$ with temperature.

Fig. 9 shows plots of the theoretical and experimental results for d.c. and a.c. resistivity versus temperature and the temperature dependence of the density of occupied acceptor states $n_s(T)$. Agreement between theory and experiment for $\rho(T)$ versus temperature, above T_0, could be obtained by using $\varepsilon_m(T)$ according to the modified Curie–Weiss law (Equation 2) instead of Equation 1. It is suggested that in this temperature region the relative permittivity value inside the depletion layer at a grain boundary consists of two parts:

1. One part is temperature-independent which represents the first part of Equation 2.
2. The second part is temperature-dependent which follows the Curie–Weiss law and represents the polarization of the residual domains which are present in the paraelectric region.

Similar assumptions have been considered by other investigators [19].

The corresponding total acceptor density N_s and the acceptor energy E_s are $(8.3\times10^{17})\,\text{m}^{-2}$ and 0.825 eV, respectively, for d.c. measurements of $\rho(T)$ and $(6.52\times10^{17})\,\text{m}^{-2}$ and 0.825 eV for a.c. measurements of $\rho(T)$. The value of E_s is quite close to the values obtained by other workers in the range 0.7–1.2 eV [3, 8, 9, 16, 36]. The value of N_s is as stated above and within the same range of other previously reported results [36] for the same materials. The width of the grain boundary layer may be estimated by using Equation 5 and has been found to be 0.3 μm; this is in agreement with the result obtained by Jonker [20].

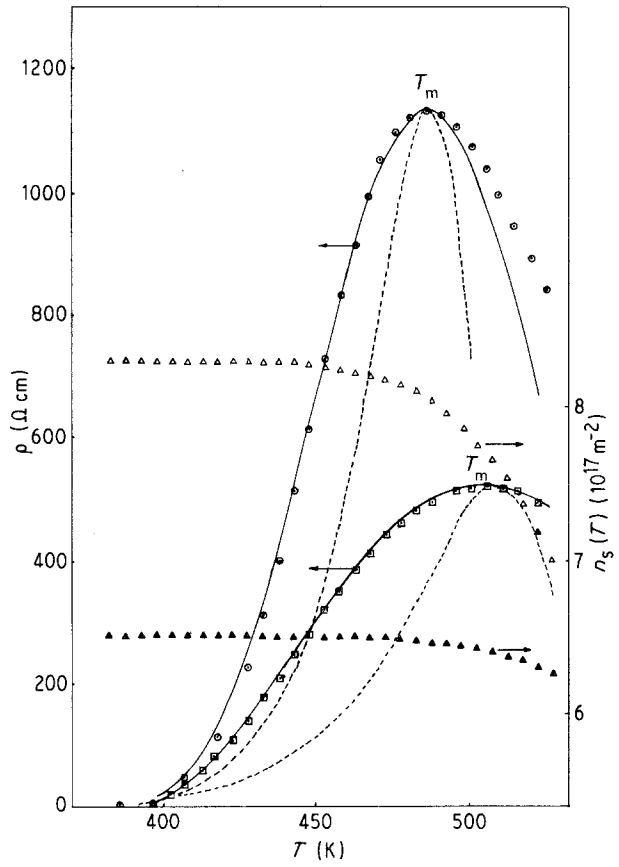

Figure 9 Temperature dependence of experimental $\rho(T)$ from (⊙) d.c. and (⊡) a.c. (1.2 kHz) measurements; theoretical $\rho(T)$ from (——) Equation 2 and (– – –) Equation 1; and density of occupied acceptor states from (△) d.c. $\rho(T)$ and (▲) a.c. $\rho(T)$.

$n_s(T)$ versus temperature (Fig. 9) shows that $n_s(T)$ is constant within the range of temperature from T_0 to 20 K below T_m; at these temperatures $n_s(T)$ is assumed to be equal to N_s. This confirms the assumption made for Equations 9 and 10. For high temperatures $n_s(T)$ decreases as the temperature increases. As a result of this behaviour $\rho(T)$ increases with increasing temperature to reach the maximum value at T_m and decrease again with further increase of temperature.

4. Conclusions

1. The contact resistances resulting from use of In–Ga and Ni electrodes are negligible when compared to those obtained with Au and Ag.

2. Complex impedance plane plot analysis is a quite useful technique for determination of the resistance of conductive grains, grain boundaries and electrode interfaces.

3. The relative permittivity of $BaTiO_3$ doped with 0.4 mol % Ho_2O_3 has been shown to obey the modified Curie–Weiss law (Equation 2).

4. Very good agreement between theory and experiment for PTCR was obtained by using Equation 2 for the relative permittivity and $E_s = 0.825$ eV, $N_s = (8.3 \times 10^{17})$ m^{-2} for d.c. measurements of $\rho(T)$ and $E_s = 0.825$ eV, $N_s = (6.52 \times 10^{17})$ m^{-2} for a.c. measurements of $\rho(T)$.

5. $n_s(T)$ is constant within the temperature range of T_0 to 20 K below T_m, and decreases for further increase of temperature.

Acknowledgements

Financial support by the research centre of College of Science Project No. Phys/1404/48 is acknowledged. Valuable discussion with Dr A. M. Hassib is appreciated.

References

1. O. SABURI, *J. Phys. Soc. Jpn* **14** (1959) 1159.
2. W. T. PERIA, W. R. BRATSCHUN and R. D. FENITY, *J. Amer. Ceram. Soc.* **44** (1961) 249.
3. W. HEYWANG, *Solid State Electron.* **3** (1961) 51.
4. O. SABURI, *J. Amer. Ceram. Soc.* **44** (1961) 54.
5. V. J. TENNERY and R. L. COOK, *ibid.* **44** (1961) 188.
6. G. GOODMAN, *ibid.* **46** (1963) 48.
7. P. K. GALLAGHER, F. SCHREY and F. V. Di MARCELLO, *ibid.* **46** (1963) 369.
8. G. H. JONKER, *Solid State Electron.* **7** (1964) 895.
9. W. HEYWANG, *J. Amer. Ceram. Soc.* **47** (1964) 484.
10. J. B. MACCHESNEY and J. F. POTTER, *ibid.* **48** (1965) 81.
11. G. T. MALLIC and P. R. EMTAGE, *J. Appl. Phys.* **39** (1968) 3088.
12. B. M. KULWICKI and A. J. PURDES, *Ferroelectrics* **1** (1970) 253.
13. C. A. MILLER, *J. Phys. D: Appl. Phys.* **4** (1971) 696.
14. P. GERTHSEN and B. HOFFMANN, *Solid State Electron.* **16** (1973) 617.
15. J. DANIELS and R. WERNICKE, *Philips Res. Repts* **31** (1976) 544.
16. H. IHRIG and W. PUSCHERT, *J. Appl. Phys.* **48** (1977) 3081.
17. R. WERNICKE, *Phys. Status Solidi (a)* **47** (1978) 139.
18. M. NEMOTO and I. ODA, *J. Amer Ceram. Soc.* **63** (1980) 398.
19. D. C. SINCLAIR and A. R. WEST, *J. Appl. Phys.* **66** (1989) 3850.
20. G. H. JONKER, in "Advances in Ceramics", Vol. 1, edited by L. M. Levinson (American Ceramic Society, Columbus, Ohio, 1981) p. 155.
21. M. KUWABARA, *J. Amer. Ceram. Soc.* **64** (1981) 639.
22. M. B. HOLMES, V. A. McCROHAN and W. Y. HOWNG, *Adv. Ceram.* **7** (1983) 146.
23. K. H. YOON, K. Y. OH and S. O. YOON, *Mater. Res. Bull.* **21** (1986) 1429.
24. H. M. AL ALLAK, G. M. RUSSELL and J. WOODS, *J. Phys. D: Appl. Phys.* **20** (1987) 1645.
25. B. S. CHIOU, *J. Mater. Sci.* **22** (1987) 3893.
26. H. F. CHENG, *J. Appl. Phys.* **66** (1989) 1382.
27. S. K. SUNDARAM, *J. Phys. D: Appl. Phys.* **23** (1990) 103.
28. I. UEDA and S. IKEGAMI, *J. Phys. Soc. Jpn* **20** (1965) 546.
29. M. KUWABARA, *Adv. Ceram.* **7** (1983) 137.
30. *Idem, Solid State Electron* **27** (1984) 929.
31. W. HEYWANG and W. WERSING, *Ferroelectrics* **7** (1974) 361.
32. H. UEOKA, *ibid.* **7** (1974) 351.
33. H. IHRIG, *Phys. Status Solidi (a)* **47** (1978) 437.
34. S. SHIRASAKI, H. HANEDA, K. ARAI and M. FUJIMOTO, *J. Mater. Sci.* **22** (1987) 4439.
35. H. M. AL-ALLAK, J. ILLINGSWORTH, A. W. BRINKMAN, G. J. RUSSELL and J. WOODS, *J. Appl. Phys.* **64** (1988) 6477.
36. H. M. AL-ALLAK, J. ILLINGSWORTH, A. W. BRINKMAN and J. WOODS, *J. Phys. D: Appl. Phys.* **22** (1989) 1920.
37. T. F. LIN and C. T. HU, *J. Mater. Sci.* **25** (1990) 3029.
38. J. ILLINGSWORTH, H. M. AL-ALLAK, A. W. BRINKMAN and J. WOODS, *J. Appl. Phys.* **67** (1990) 2088.
39. H. M. LANDIS, *ibid.* **36** (1965) 2000.
40. H. S. MAITI and R. N. BASU, *Mater. Res. Bull.* **21** (1986) 1107.

41. S. O. YOON, M. J. JUNG and K. H. YOON, *Solid State Commun.* **64** (1987) 617.
42. K. H. YOON, H. S. PARK, S. O. YOON and M. I. SONG, *J. Korean Ceram. Soc.* **26** (1989) 73.
43. *Idem, J. Mater. Sci. Lett.* **8** (1989) 1442.
44. A. AMIN, *Ferroelectrics* **87** (1988) 41.
45. L. A. XUE, Y. CHEN and R. J. BROOK, *J. Mater. Sci.* **7** (1988) 1163.
46. M. A. A. ISSA, N. M. MOLOKHIA and S. A. NASSER, *J. Phys. D: Appl. Phys.* **17** (1984) 571.
47. N. M. MOLOKHIA, M. A. A. ISSA and S. A. NASSER, *J. Amer. Ceram. Soc.* **67** (1984) 289.
48. C. G. KOOPS, *Phys. Rev.* **83** (1951) 121.
49. R. FLORES-RAMIREZ, A. HUANOSTA, E. AMANO, R. VALENZUELA and A. R. WEST, *Ferroelectrics* **99** (1989) 195.
50. G. RUPPRECHT and R. O. BELL, *Phys. Rev.* **135** (1964) A748.

Received 12 March
and accepted 25 July 1991